Robotics and Autonomous Systems 164 (2023) 104407

Contents lists available at ScienceDirect

Robotics and Autonomous Systems

journal homepage: www.elsevier.com/locate/robot

Force control of lightweight series elastic systems using enhanced disturbance observers

Andrea Calanca *, Enrico Sartori, Bogdan Maris

Department of Computer Science, University of Verona, Strada Le Grazie 15, 37134 Verona, Italy

ARTICLE INFO

Article history:
Received 9 September 2021
Received in revised form 30 December 2022
Accepted 14 March 2023
Available online 17 March 2023

Keywords:
Force control
Series elastic actuators
Disturbance observers

ABSTRACT

This paper analyzes the control challenges associated to lightweight series elastic systems in force control applications, showing that a low end-point inertia can lead to high sensitivity to environment uncertainties. Where mainstream force control methods fail, this paper proposes a control methodology to enhance the performance robustness of existing disturbance observers (DOBs). The approach is validated experimentally and successfully compared to basic control solutions and state of the art DOB approaches.

© 2023 Published by Elsevier B.V.

1. Introduction

The deliberate introduction of compliance has probably been one of the main shifts in robot design during the last two decades [1,2]. Since the introduction of series elastic actuation (SEA), robot compliance has been often implemented at the joint level, i.e. by adding a deformable element between the motor and the link, leading to accurately sense and control forces/torques at each robot joint [3–5]. Such a solution is considered a fundamental perspective change with respect to older "the stiffer the better" paradigm or with respect to previous compliance implementations such as the "remote center of compliance" [6,7].[1] Following the success of joint-level compliance, link-level compliance has been introduced by exploiting the inherent flexibility of robotic links and using it as a force feedback signal [8,9]. Link-level compliance retains control advantages similar to joint-level compliance but avoids the need of designing and arranging custom springs in series to the motor. Under certain assumptions (lightweight links subject to small deformations) link compliance can be modeled similarly to joint compliance [10–12] and this led us to conceive the name "Series Elastic Link" (SEL) in analogy with the term "Series Elastic Actuator" [8,9]. Exploiting link compliance can benefit a variety of force control applications. As an example, surgical robots for minimally invasive surgery apply forces trough *low-inertia* laparoscopic tools which can be reasonably modeled as lightweight flexible links. Such tools can be instrumented to provide deformation measurements [13], as shown in Fig. 1a. Other examples can be wearable robotic applications such as robotic orthoses and prostheses where *lightweight* requirements may lead to flexibilities in the robot structure. Fig. 1b reports an example of 3D printed upper limb orthosis where robot forces are transferred to the human through a *lightweight* plastic structure [14,15].

This paper considers such kind of robot structures where flexible links *with low inertia* are used to transfer forces to a human or to an environment. The first contribution is to highlight and formally state the force control challenges associated with these kind of systems which are due to high sensitivity to human/environment uncertainties. The second contribution is a force control design able to enhance robustness to human/environment uncertainties. This design is based on an novel disturbance observer (DOB) architecture with an inner feedback able to guarantee a dynamics quite insensitive to the interacting environment. Thanks to such inner feedback, the outer DOB can assume a nominal model which is always a good description of the real plant (which includes the inner feedback), leading to higher stability robustness. Differently, other DOB approaches may lead to a dramatic mismatch between the nominal plant assumed by the DOB and the actual plant. This can cause unstable or oscillating behaviors. In these solutions a "nominal environment" is implicitly or explicitly assumed and interacting with an environment which is far from the nominal one causes a large mismatch between the actual plant and the nominal plant assumed by the DOB. For example, the DOBs analyzed in [16] consider an infinitely stiff environment. As a consequence, they work bad in soft environments. Conversely, the DOB proposed in [17] considers an infinitely soft environment and behaves bad in stiff environments.

The paper is organized as follows. Section 2 summarizes the past work on force control of flexible links and series elastic systems summarizing existing modeling and control approaches. In

* Corresponding author.
E-mail address: andrea.calanca@univr.it (A. Calanca).

[1] The "Remote center of compliance" refers to a mechanical architecture where a flexible element is arranged at the end-effector of a rigid position-controlled robot without providing any force sensing or feedback.

https://doi.org/10.1016/j.robot.2023.104407
0921-8890/© 2023 Published by Elsevier B.V.

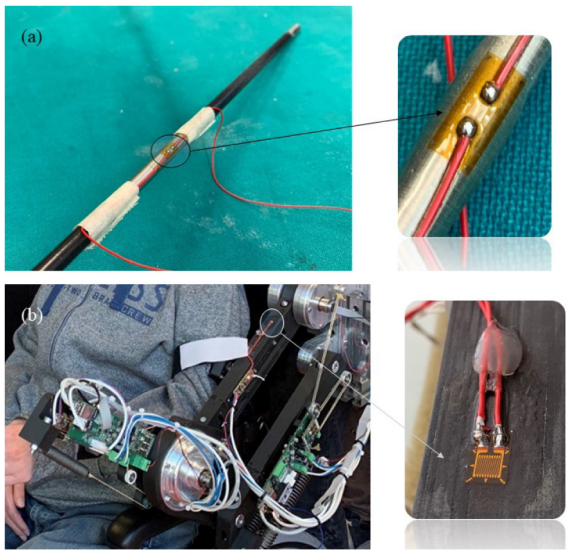

Fig. 1. Example of robotics applications involving flexible links with low end point inertia: (a) a laparoscopic tool used in surgical robots and (b) a 3D printed upper limb orthosis. In both the cases the flexible link is instrumented to provide deformation measurements.

this section the reader will understand that even if the proposed methodology is applied here to the specific case of lightweight flexible links, our analysis is valid for the more general case of series elastic systems characterized by low end-point inertia. Section 3 expands on control issues related to low end-point inertia and theoretically motivates the proposed control architecture. Section 4 describes the experimental validation and the comparison made with state of the art DOBs. Section 5 reports our conclusions and plans for future work.

2. Background

2.1. Flexible links

Controlling robots with flexible links has a long history dating back to mid-80s [18–21]. Most of existing works deal with the problem of position control where the main objective is to control the link end-point position while suppressing vibrations due to the cantilever beam dynamics [22–28]. Even if continuum mechanics models exist – derived using the Lagrangian formalism and based on partial differential equations along time and space coordinates [26,29–33] - the very most of existing works consider linearized models along a defined spatial coordinate. They use time–space separation to define the frequency relation between the motor input torque and the link position or orientation at the selected spatial coordinate [18,20,21,34–40]. These works introduces a further approximation where the infinite-order expression coming from time-domain motion equation is trunked – often to the second order – leading to a dominant dynamics amenable to those of series elastic systems.

The main objective of all these works is position control, however in certain cases the link strain – which represents a direct measure of the transmitted force – is measured and fed back to improve vibration suppression [30,33,41,42]. Force control has been rarely considered as an explicit objective. To the best of author knowledge the only existing force control approaches applied to flexible links are [10,43–50]. Interestingly, most of these works considers a second order system approximation leading exactly to the model of a series elastic system. Even more important, none of these solutions has been conceived to face well-known force control challenges such as the *sensitivity to environment uncertainties*.

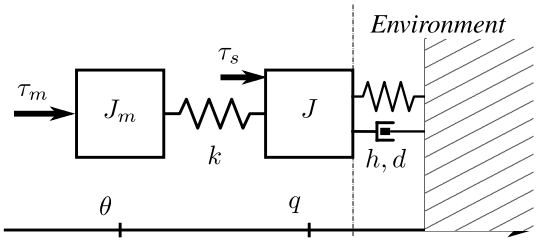

Fig. 2. A model for a series elastic system interacting with an environment with stiffness h and damping d.

2.2. Modeling series elastic systems

The dynamics of a rotary series elastic system can be modeled as represented in Fig. 2 where angular variables (angles and torques) are translated into linear equivalents (linear positions and forces). The variable θ represents the motor position, q is the environment position, τ_m is the motor input torque (proportional to the current), τ_s is the spring torque, τ_e is the torque exerted by the environment, J_m is the reflected motor-gear inertia, k is the torsional stiffness of the series elastic element and J represents the robot end-point inertia. As the overall system to control includes the environment [51,52], d and h represent the environment damping and stiffness, respectively. This model represents a generic series elastic system and can be used either to describe series elastic actuation, flexible links or stiff force control applications. In the latter case the force sensor is modeled as an extremely high series stiffness. In the case of lightweight links subject to small perturbations, a modeling equivalence between rotary SEAs and flexible links exist [8,10–12]. This can be derived by introducing an equivalent torsional stiffness which describes the link bending stiffness. Such stiffness explains the relation between the link deflection (measured as a joint displacement angle) and the external force F applied at the tip (causing a joint torque), as represented in Fig. 3. The equivalent stiffness can be computed considering the link material and geometry as

$$k = \frac{3IE}{L^2} \tag{1}$$

where E is the Young modulus of the beam material, I represents the area moment of inertia of the beam section and L is the link length.

In the light of these considerations, the dynamics of a generic series elastic system interacting with an environment can be expressed as

$$J_m\ddot{\theta} = \tau_m - \tau_s \tag{2}$$

$$\tau_s = k(\theta - q) \tag{3}$$

$$J\ddot{q} + d\dot{q} + hq = \tau_s - \tau_e. \tag{4}$$

One can observe that motor-side damping is ignored in this work. Not considering damping in Eq. (2) does not significantly alter the location of poles [52] and put us in a worst case condition for stability robustness. Indeed motor-side damping positively affects the system stability robustness and is often used in the case of non-collocated dynamics and/or when interacting with unknown environments [53,54]. For example, passivity-based control – which is often used to guarantee stability when interacting with passive environments – requires motor-side dissipation [55]. Not considering damping in Eq. (2) makes it clear that our analysis and results do not rely on such stabilizing effects given by motor-side damping.

In order to design a force control algorithm, the plant transfer function $F(s)$ must include the environment and has the motor

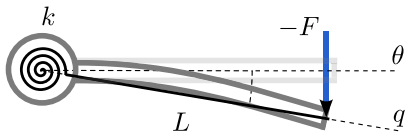

Fig. 3. An elastic link model where the link bending stiffness is translated into an equivalent torsional stiffness. The force F as exerted by the environment is such that $-\tau_e = -LF$ where L is the link length.

torque τ_m as input and the torque τ_s as output [17,52]. The latter can be measured by considering the deformation of a spring, a flexible link or a force sensor, depending on the specific system. As detailed in [52] such transfer function can be expressed as

$$F(s) = \frac{\tau_s(s)}{\tau_m(s)} = \frac{E(s)}{(E(s)+r)\frac{J_m}{k}s^2 + E(s)} \tag{5}$$

where

$$E(s) = \frac{J}{h}s^2 + \frac{d}{h}s + 1 \tag{6}$$

is the environment transfer function and $r = \frac{k}{h}$ is the ratio between robot and environment stiffnesses.

To prepare for the analysis in Section 3 it is worth to summarize some previous findings regarding the transfer function $F(s)$:

(1) The transfer function $F(s)$ is characterized by an unitary static gain, two zeros and four poles.
(2) The zeros location is centered around the frequency $\omega_E = \sqrt{h/J}$.
(3) The poles are a more complex function of both robot and environment parameters and they typically gives rise to two distinct resonances. In particular, a pair of poles is centered around ω_{p1} while another pair is centered around ω_{p2} where

$$2\omega_{p1,2}^2 = \omega_{SE}^2 - \tilde{\omega}_E^2 \mp \sqrt{(\omega_{SE}^2 - \tilde{\omega}_E^2)^2 + 4r\omega_E^2\omega_{SE}^2}. \tag{7}$$

The quantity $\omega_{SE} = \sqrt{k/J_m}$ is the natural resonance of the series-elastic system coupled with an infinitely rigid environment and only depends on actuator parameter. Also we define $\tilde{\omega}_E^2 = \omega_E^2(1+r)$.
(4) It can be shown that one resonance is always below ω_E leading the force dynamics $F(s)$ to possibly exhibit a *phase drop* below ω_E. Such phase drop has been documented in the literature even using a more complex model [56].

See [52] for a more detailed explanation of the above points.

2.3. Controlling series elastic systems

In general, force control is recognized as a challenging problem which often requires advanced solutions. In the case of series elastic systems the main reported challenges are related to uncertainties coming from the human/environment dynamics which enters in the force closed-loop affecting both performance and stability. Several force control applications have been described using models similar to (2)–(4) leading to the transfer function $F(s)$ in (5) and thus explaining the sensitivity to environment dynamics, i.e. to the environment transfer function $E(s)$. Several force control approaches have been proposed in the last two decades to enhance robustness to environment uncertainties, most of them explicitly focused on the case of SEAs. In particular, we have seen the application of different control techniques such as disturbance observers (DOBs) [57–59], acceleration feedback [3,52,60], sliding-mode control [61,62], adaptive control [63–66] and H_∞ control [67], just to cite the most popular. Conversely, very few advanced control approaches have been proposed for the case of flexible links. The few existing works are limited to simple control architectures, mainly proportional control [30,44,45]. However, thanks to the modeling equivalence highlighted before, the approaches conceived for SEA can be in principle applied to the case of flexible lightweight links.

Before proceeding it is worth mentioning that among existing force control algorithms, DOBs represent a well-liked mainstream solution with dozens of papers published in recent years. DOBs allow to estimate disturbances between the actual system and a chosen nominal model, and use this estimate as a cancellation signal to better follow the reference [68]. A typical control architecture based on DOB is shown in Fig. 5 where $P_n(s)$ represents the plant nominal model, $\Delta(s)$ represents the plant uncertainties and $Q(s)$ is a frequency filter allowing for nominal model inversion. The signal $\hat{d}$ represents the disturbance estimation which is considered as additive. In DOBs architectures, such estimation is negatively fed back attempting to cancel the "real" disturbance. However, in typical force control applications there is not a real additive disturbance and the signal $\hat{d}$ do not always have an intuitive physical meaning. DOB performance and stability depend on the choice of both $Q(s)$ and $P_n(s)$. According to existing results the system "may become unstable when the Q filter is designed based on the stability conditions with poor knowledge of uncertainties" and to avoid such case, the cutoff frequency of the filter "needs to be decreased to improve the robustness of DOB, which may results in deterioration of the performance" [69]. In general, DOBs can be used in two *configurations*: an open-loop configuration, as the one in Fig. 5 - where the DOB is applied to the plant- and a closed-loop configuration-where the DOB is applied to the closed-loop system composed by the plant and the controller (the controller dynamics is included into the DOB nominal model) [16,17,57,59]. Two *nominal models* has been proposed in the literature, a second order nominal model which assumes a nominal infinitely rigid environment and a third order nominal model which assumes a nominal infinitely soft environment (i.e. the environment is supposed to do not apply any force) [17]. In the latter case the signal $\hat{d}$ estimates the interaction forces with the real environment, in the former case the interpretation of $\hat{d}$ is less intuitive (and is related to the environment acceleration). Two DOB configurations combined with two nominal models give rise to four possible combinations. Three of these combinations have been reported in the literature and the only existing comparison involves just two of them [16].

The FORECAST project is funded by EU in order to provide a standardized comparison of force control algorithms. Preliminary (and unpublished) results confirm that in the case of low end-point inertia existing DOB architectures fail to guarantee suitable performance robustness. These findings motivate the work described in this paper and are reported within the experimental results in Section 4.

3. Proposed control methodology

This section describes the proposed control methodology. The problem is introduced in Section 3.1, the methodological approach is theoretically motivated in Section 3.2 while issues and limitations are discussed in Section 3.3. Finally, an enhanced DOB architecture is proposed in Section 3.4.

3.1. Control implications of low end-point inertia

In order to introduce the implications of low end-point inertia in force control applications, we report in Fig. 4 a set of Bode plots of the transfer function $F(s)$. Each plot is related to a specific

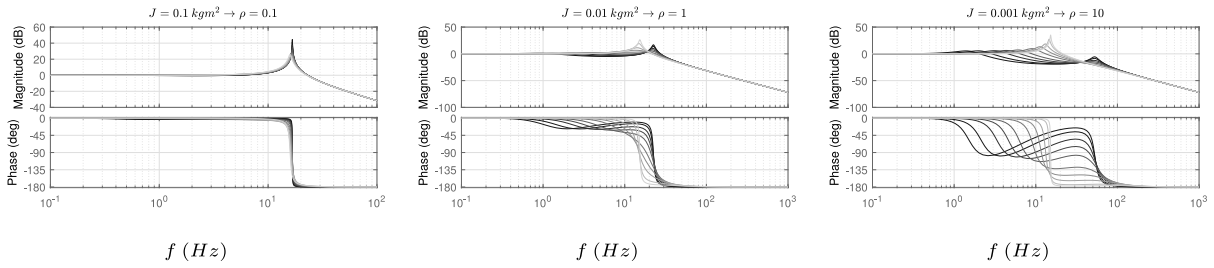

Fig. 4. Bode plots of $F(s)$ considering the interaction with different environments. Each Figure is related to a specific value of J. Within the same figure, plots with different gray tones are related to different environment stiffness, from $h = 1$ N m/rad (darker line) to $h = 1000$ N m/rad (lighter line). For simplicity we considered a damping value d such as the E(s) is critically damped. The actuator inertia $J_m = 0.01$ kg m^2 and the link stiffness $k = 100$ N m/rad are chosen with the same order of magnitude of our prototype and are constant in all plots.

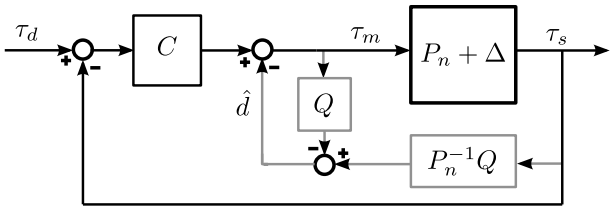

Fig. 5. Force control based on DOB in open-loop configuration. The DOB is highlighted in gray.

value of the parameter J and considers a wide range of human/environmental stiffness: lines with different gray tones are related to different environment stiffness, from $h = 1$ N m/rad (darker line) to $h = 1000$ N m/rad (lighter line). One can observe that as the parameter J gets lower, the system to control displays higher sensitivity to environmental stiffness: in the right plot the frequency responses of $F(s)$ are significantly different one from each other. Differently, in the left plot, where the end-point inertia J is higher, such sensitivity cannot be observed. In the following we formally motivate this phenomena which may affect the control performance and stability.

In this paper we highlight the importance of the parameter

$$\rho = \frac{J_m}{J} \tag{8}$$

which defines the ratio between the actuator inertia and the end-point inertia, given in our case by the link inertia. Now, if we arrange Eqs. (2), (3) and (4) in

$$\frac{J_m}{k}\ddot{\tau}_s + (1+\rho)\tau_s = \tau_m + \rho(hq + d\dot{q}) \tag{9}$$

we find out that ρ modulates the effect of the environment dynamics (4) on the output force dynamics $F(s)$. Indeed, when ρ tends to zero the dynamics of τ_s is no longer influenced by environmental parameters (stiffness h and damping d). This explains why the Bode plots shown in Fig. 4 on the right are very sensitive to environmental stiffness, whereas the plots on the left are quite insensitive. Of course, in the case of lightweight links the parameter ρ may become very high because J may assume very low values. Therefore the system may become very sensitive to the environment and difficult to control in force. In particular, it cannot tolerate high force gains [51,70]. Unfortunately, a low gain controller cannot properly dominate the environment uncertainties in the right plot of Fig. 4. Thus, obtaining a nice interaction with both stiff and soft environments is not trivial.

3.2. Enhancing robustness to environment uncertainties

In the light of the previous considerations, controlling the deformation of very lightweight links represents a challenging task: performance may change and degrade depending on the specific environment. Coincidentally, several existing algorithms (originally conceived for SEA) cannot be successfully applied to elastic links. For example, some algorithms require information on the load side acceleration $\ddot{q}$, i.e. the acceleration of the inertia J in Fig. 2, which is not available with elastic links.[2] This prevents the application of certain force control algorithms such as the ones described in [3,61,71–73]. Similarly, force control algorithms based on DOBs, which are often used in the SEA literature, tend to behave badly when the parameter J is low, as we show in Section 4.

Differently from existing approaches, in this paper we highlight the potential of a simple control strategy and theoretically motivate its effectiveness in reducing the sensitivity to environment uncertainties. Such control strategy can be combined with existing DOB architectures in order to enhance their robustness properties, as detailed in Section 3.2. In particular, we show that robustness to environment uncertainties can be enhanced by closing a high-gain derivative loop on the force signal, as represented in the simple architecture of Fig. 6, where k_d is a sufficiently high derivative gain. This section shows that, despite environment uncertainties, the system $W(s)$ seen from the external terminals $(u,\ \tau_s)$ can be well approximated by a first order dynamics with unitary static gain and a single pole located in $-1/k_d$. This is exemplified in Fig. 7 which reports the Bode plots of the transfer function $F(s)$ (gray lines) for different values of environment stiffness and the related Bode plot of the transfer function $W(s)$ (red lines). It is immediate to notice that the uncertainties due to the environment dynamics are impressively reduced: the red diagrams are extremely close to each others and, irrespectively of the specific environment stiffness, all describe a similar first order dynamics. As a consequence, while controlling $F(s)$ may represent a challenging task, controlling $W(s)$ becomes simpler. The residual uncertainty due to the environment is extremely low and – within a large frequency range – the phase is above $\pi/2$. In the following we demonstrate why the system dominant dynamics reduces to such a single pole dynamics, and under which conditions the pole location is close to $-1/k_d$.

To this aim, let us consider the root locus of the inner derivative loop as represented in Fig. 8. The transfer function $F(s)$ is always characterized by two zeros and four poles – often complex conjugate – which give rise to the resonance peaks as shown in Figs. 4 and 7. An additional zero is introduced by the derivative feedback. Being four poles and three zeros, three poles are attracted to the zeros and the remaining one goes toward infinity along the real axis. For sufficiently high values of the loop gain k_d such pole goes to the high spectrum and can be neglected.

[2] Even if the load position can be reconstructed from (3) as $q = \theta - \frac{\tau_s}{k}$, computing the load acceleration implies a double differentiation of a torque signal which is practically unfeasible because of electrical noise amplification.

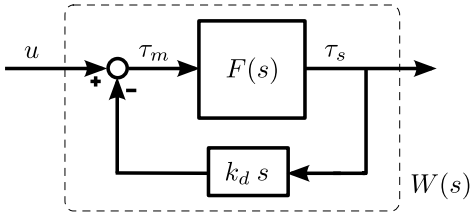

Fig. 6. Block diagram representation of the inner derivative loop arranged on the feedback path.

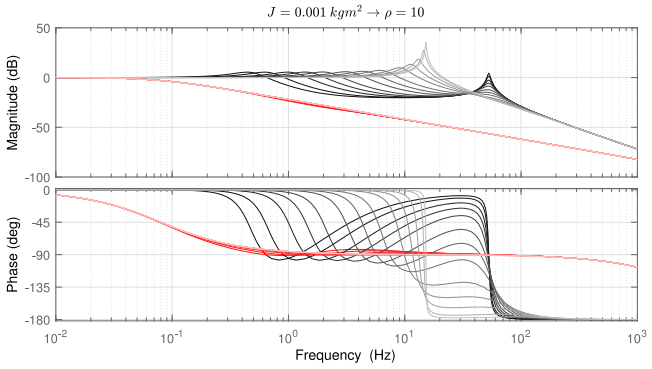

Fig. 7. Bode plots of $F(s)$ (gray) and $W(s)$ (red) with $k_d = 2$ considering different environmental stiffness from $h = 1$ N m/rad (dark lines) to $h = 1000$ N m/rad (lighter lines). The value $J = 0.001\ Kgm^2$ is chosen to represent the case of a lightweight link in contact with a soft environment. Without lack of generality the environment is considered critically damped. The actuator inertia $J_m = 0.01$ kg m^2 and the link stiffness $k = 100$ N m/rad are chosen with the same order of magnitude of our prototype. (For interpretation of the references to color in this figure legend, the reader is referred to the web version of this article.)

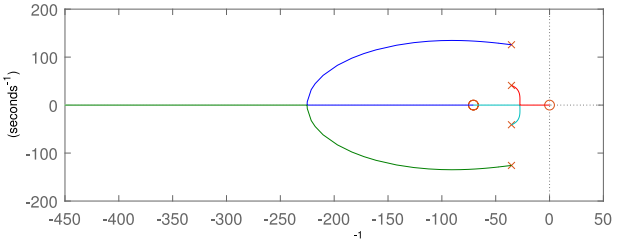

Fig. 8. A representation of typical root locus diagram related to $F(s)$ with inner derivative feedback k_d. As k_d increases three poles move toward the zeros and the fourth pole goes to the high spectrum.

The dominant system dynamics is given by the pole attracted toward the zero on the origin, while the remaining two pole-zero couples concur to non-dominant higher order dynamics. Such dynamics are non-dominant not only because they are in the higher frequency spectrum but mainly because they are couples of zeros and poles which mutually abate their effects. Indeed, for sufficiently high values of the loop gain k_d, such poles are located sufficiently close to the zeros. Instead, the zero in the origin does not appear in $W(s)$, thus avoiding any cancellation with the low frequency pole. This is obtained by arranging the derivator on the feedback path. If the derivator block was set on the forward path some of the following results would be different. In particular a zero in the forward path may let the higher frequency dynamics (which are sensitive to environment uncertainties) to appear in the responses. Thus, to observe the aforementioned robustification is essential to insert the derivative action in the feedback and not in the forward path. In this way the zero given by the derivator attracts the low-frequency pole toward the origin without appearing in the closed-loop transfer function.

In the following we show that the location of the dominant pole is often well approximated by the value $-1/k_d$. This can be more easily explained if we neglect the non-dominant dynamics in $F(s)$ given by the two couples of poles and zeros that, for sufficiently high values of k_d, cancel out their effects. Discarding such poles and zeros, $F(s)$ can be reasonably approximated to

$$\tilde{F}(s) = \frac{\omega_n^2}{s^2 + 2\xi\omega_n s + \omega_n^2} \tag{10}$$

where ω_n represent the location of the low frequency poles in $F(s)$, i.e. $\omega_n = \omega_{p1}$ as defined in (7), and ξ is the related damping. As a preliminary consideration let us observe the plots in Fig. 4: the location of such low frequency poles is always above a certain threshold ω_{th}, such that $\omega_n > \omega_{th}$, which in the case of Fig. 4 can be evaluated around 1 Hz.[3] Then, let us compute the closed-loop dynamics of the system shown in Fig. 6, obtained by closing a derivative feedback around $\tilde{F}(s)$,

$$\tilde{W}(s) = \frac{\omega_n^2}{s^2 + (k_d\omega_n^2 + 2\xi\omega_n)s + \omega_n^2} \tag{11}$$

and let us compute the closed-loop poles as

$$s_{1,2} = \frac{-(k_d\omega_n^2 + 2\xi\omega_n) \pm \sqrt{(k_d\omega_n^2 + 2\xi\omega_n)^2 - 4\omega_n^2}}{2}. \tag{12}$$

As a first step, let us analyze the location of these poles for high values of the parameter ω_n. According to the following theorem, which considers the limit condition $\omega_n \rightarrow +\infty$, the low frequency pole is located exactly in $-1/k_d$.

Theorem 1. *Let us consider a generic second order system in the form (10) and the feedback architecture in Fig. 6 where $F(s)$ is replaced by $\tilde{F}(s)$, then the location of the dominant pole s_1 in (12) tends to $-\frac{1}{k_d}$ for $\omega_n \rightarrow \infty$, irrespectively of the damping factor ξ. In particular*

$$\forall\xi \quad \lim_{\omega_n\to\infty} s_1 = -\frac{1}{k_d} \tag{13}$$

Proof. Let us rewrite the expression for s_1 in (12) as

$$s_1 = \frac{1}{2}(a - b) = \frac{1}{2}\frac{(a^2 - b^2)}{a + b} \tag{14}$$

where $a = \sqrt{(k_d\omega_n^2 + 2\xi\omega_n)^2 - 4\omega_n^2}$ and $b = (k_d\omega_n^2 + 2\xi\omega_n)$. By substituting a and b in (14) and collecting ω_n^2 at both the numerator and denominator we have

$$s_1 = \frac{1}{2}\frac{-4}{\sqrt{(k_d + 2\xi/\omega_n)^2 - 4/\omega_n^2} + (k_d + 2\xi/\omega_n)}$$

which easily leads to (13). Thus, irrespectively of the kind of pole of the original system (i.e. for any value of the damping factor ξ) the location of the closed-loop dominant pole s_1 tends to $-\frac{1}{k_d}$. ■

As a second step we analyze what happens for low values of ω_n. Fig. 9 reports the closed-loop pole location s_1 as a function of the independent variable ω_n, for different values of the derivative gain k_d. It can be observed that starting from a certain threshold ω_{th}, such that $\omega_n > \omega_{th}$ the pole location s_1 is rather insensitive

[3] Of course depending on the application different threshold values can be found. For a given application one should consider the robot model and a set of environment of interest by defining the maximum and minimum stiffness (and eventually damping) coefficients. Then, the pole located at lowest frequency defines the threshold ω_{th}.

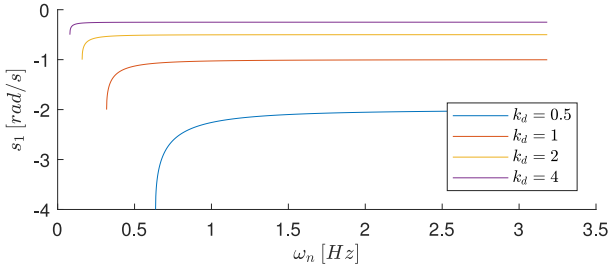

Fig. 9. Location of the closed-loop dominant pole s_1 as a function of the location of open loop low frequency poles.

to variations of the independent variable ω_n, especially for high values of k_d. As an example, considering $\omega_{th} = 1$ Hz and $k_d \geq 1$, it is possible to observe that the location of the closed-loop pole s_1 is constant, meaning that it does not depend on the location of the open-loop poles ω_n. Formally, we have that $\frac{ds_1}{d\omega_n} \simeq 0$ whenever $\omega_n > \omega_{th}$. Consequently, the closed-loop pole location will not change so much between the case $\omega_n = \omega_{th}$ and $\omega_n \to \infty$, and within this range is always close to $-1/k_d$, accordingly to Theorem 1. As shown in Fig. 9, this invariance holds only for a sufficiently high derivative gain; in our case, where $\omega_{th} = 1$ Hz, a gain $k_d = 1.0$ or higher definitely guarantees such invariance propriety. It is exactly such a property that explains why the resulting closed-loop system is insensitive to the environment dynamics (and related uncertainties). Indeed, we remind that ω_n represents the location of a pole in $F(s)$ which is affected by the environment dynamics. Fig. 9 shows that for a sufficiently high value of k_d this pole location ω_n, which depends on the environment, does not alter the location of the dominant pole s_1 in $W(s)$, thus guaranteeing the aforementioned robustness propriety.

3.3. Tuning issues and trade-offs

The previous section theoretically justifies why a sufficiently high derivative gain can remove most of the environment uncertainties in force control applications. Unfortunately, in practice, a very-high derivative gain may be a non-viable solution because of two reasons. The first is noise in the force/torque signal, which may be seriously amplified by derivative processing. The second is because a too high derivative gain leads the dominant closed-loop pole to locate in the very low spectrum (close to $-1/k_d$). Then, to obtain a reasonable closed-loop bandwidth, a high-gain outer controller may be required. Unfortunately, specific gain limits have been highlighted in the literature for force control applications due to non collocation, limited actuator bandwidth and digitalization effects [18,74–76].

In conclusion, if a higher k_d allows higher robustness, in practice it also leads to lower closed-loop bandwidth and to higher noise in the system. Thus, the designer has to find the proper trade-off between robustness (exploiting the above claimed proprieties of derivative feedback) and performance. In light of this, a moderately-high derivative gain can be considered a convenient choice. Fig. 10 shows the Bode plots of $F(s)$ and $W(s)$ related to different choices of k_d showing that, in many scenarios, uncertainty can be reduced even using a moderately-high gain. In particular, the choices in the upper plots are non-viable in our physical testbed while the lower plots represent reasonable trade-offs where the (small) residual uncertainties due to the environment can be further reduced by designing a robust outer loop, as explained in the next section.

3.4. A DOB architecture with enhanced robustness

This section proposes a two layer control architecture that combines the inner derivative feedback with an outer robust controller based on open-loop DOBs, as represented in Fig. 11. Nothing prevents the choice of a closed-loop DOB [16]. The underlying idea is that system uncertainties are managed in two stages: first, the inner derivative loop reduces the uncertainties bringing the system to a well-defined dominant dynamics, then, the residual uncertainties are handled using a DOB. Such DOB is designed based on the dominant dynamics of $W(s)$ resulting from the inner derivative loop and the specific choice of k_d. According to the considerations in the previous section, the dominant dynamics of $W(s)$ can be always approximated to a single pole located in $-1/k_d$, independently of the environment. Thus, it is possible to write a nominal plant model as

$$P_n(s) = \frac{1}{k_d s + 1} \tag{15}$$

without knowledge or assumptions on the environment parameters. This allows to implement the control architecture in Fig. 5 where $Q(s)$ is a first order low-pass filter. Differently from other DOB implementations, the inner derivative feedback allows the actual plant to be close to the nominal one even in different environment conditions. As a consequence, improved stability margins and performance are expected with respect to existing DOB implementations.

4. Experimental results

To validate our theoretical results a single-DOF elastic link prototype is implemented using a plastic hollow tube with an outer diameter $D = 32$ mm, an inner diameter $d = 30$ mm and a length of $L = 300$ mm. The tube material is polyethylene which is characterized by a Young's modulus of about 800 MPa. According to Eq. (1) this should lead to an equivalent torsional stiffness k of about 300 N m/rad.[4] The link deformation is measured using a pair of strain gauges connected to a custom electronic board including a Wheatstone bridge and amplification and filtering stages. The instrumented plastic link has been mounted on the mechanical setup shown in Fig. 12, which includes a geared motor M and a commercial torque sensor T which is used only for strain gauges calibration. System parameters have been estimated using a procedure similar to the one described in [77] as $J_m = 0.0208$ kg/m^2 and $k = 240$ N m/rad. The link inertia is estimated as $J = 0.0003$ kg/m^2 leading to a high value for the parameter $\rho = 69.3$. Coulomb and viscous frictions are identified and software compensated. Control algorithms are implemented on a standard PC where the control process runs at a 5 kHz soft real-time frequency and communicates with the motor drive and the sensor electronics via EtherCat protocol at the same rate. A frequency limit of 2 kHz given by our ADC modules determines the signal sampling frequency in spite of the higher capabilities of the computational system. Controllers are implemented in C++ within the Series Elastic Library architecture (http://metropolis.scienze.univr.it/altair/selib/). All the controllers are tested in two different environment conditions. A rigid metal plate *RP*, shown in Fig. 12, is used to implement a stiff environment condition while a soft sponge *SS* is used to implement a soft environment condition. All the controllers are implemented considering an additional static feed forward action to obtain null static error.

[4] As explained in Section 2.2 the stiffness k can be interpreted as an equivalent torsional representation for the link bending stiffness. Therefore, it should not be confused with the torsional stiffness of the plastic tube along is principal axis.

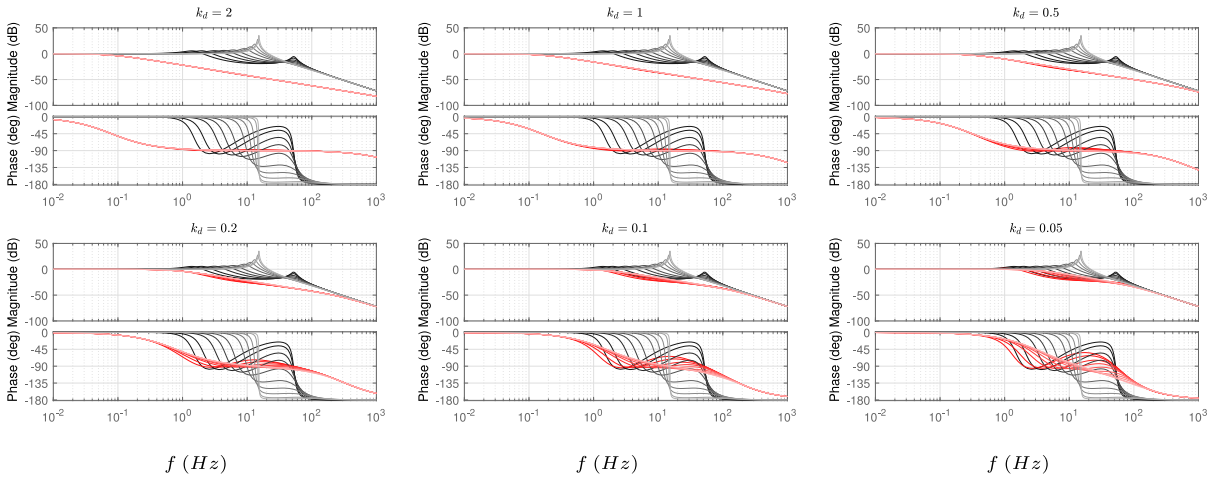

Fig. 10. Bode plots of $W(s)$ for different choices of the derivative feedback gain k_d. Each plot shows the transfer function $F(s)$ with different gray tones for different environment stiffnesses, from $h = 1$ N m/rad (darker line) to $h = 1000$ N m/rad (lighter line). The related closed-loop functions $W(s)$ are plotted in different tones of red. The actuator inertia $J_m = 0.01$ kg m^2, the link inertia $J = 0.001$ kg m^2 and the link stiffness $k = 100$ N m/rad are chosen with the same order of magnitude of our prototype and are constant in all plots. (For interpretation of the references to color in this figure legend, the reader is referred to the web version of this article.)

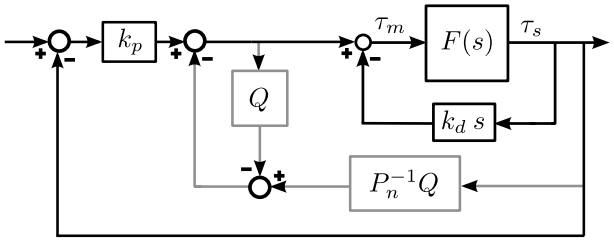

Fig. 11. Force control schema that combines the inner derivative feedback of Fig. 6 with an outer open-loop DOB. The DOB is highlighted in gray.

Table 1
Control tuning.

Control tuning	
PD	$k_p = 4,\ k_d = 0.04$
PD-overdamped	$k_p = 4,\ k_d = 0.2$
PinnerD	$k_p = 4,\ k_d = 0.2$
DOB2 OL	$k_p = 4,\ k_d = 0.2,\ \omega_q = 2\pi 0.5$
DOB2 CL	$k_p = 4,\ k_d = 0.2,\ \omega_q = 2\pi 0.5$
Enhanced-DOB	$k_p = 4,\ k_d = 0.2,\ \omega_q = 2\pi 18$

4.1. Comparison with basic force control algorithms

As a first step, we consider the architecture in Fig. 6 with inner derivative action on the backward path (as represented in Fig. 6) and outer proportional control. This architecture – that we call PinnerD – is compared with a standard proportional–derivative (PD) control, with derivative action on the forward path.

The PD controller is tuned, considering a stiff environment condition, to theoretically obtain a critically damped closed-loop response with bandwidth around 40 Hz. The PinnerD controller is tuned following the consideration in Section 3.3. First, the derivative gain is tuned as high as possible without introducing noise. We found a reasonable trade-off by low-pass filtering the derivative signal and by using $k_d = 0.2$.[5] Then we raise the outer proportional gain up to the maximum value allowed by our implementation. All gain values are reported in Table 1.

Fig. 14 shows the torque tracking response of PD and PinnerD controllers where the torque reference τ_{ref} is shown in blue and the actual response τ_s in red. The considered torque reference is a sweep signal reaching a 5 Hz frequency after 60 s. For the PinnerD case, we also reported the expected response τ_{exp} in black, computed considering the dominant dynamics of $W(s)$ as in (15). According to our expectations, the PD controller leads to higher bandwidth but exhibits different responses in different environments showing a resonant response when interacting with the soft sponge. Differently, the PinnerD controller exhibits more similar responses even if some discrepancies can be observed with respect to the expected behavior (in black) especially in higher frequencies. For the sake of completeness we also tested a PD controller tuned with the same gain values (and derivative filtering) used for the PinnerD architecture, to verify the conjecture that a higher derivative gain could properly dampen the response in soft environments. Fig. 14 shows that this is not the case. As justified previously, this is because the PD controller introduces an additional zero in the forward path altering the results presented in Section 3.2.

4.2. Comparison with existing DOB architectures

In this step, we implemented four DOB architectures, based on the combination of two configurations (open-loop and closed loop) and two nominal plants (second order and third order), as explained in Section 2. The following controllers are implemented:

(1) DOB2-OL: An open-loop DOB architecture, as represented in Fig. 5, using a second order nominal plant in the form

$$P_n^{2nd}(s) = \frac{1}{\frac{J_m}{k}s^2 + \frac{d_m}{k}s + 1}, \tag{16}$$

where d_m is the motor damping. Such nominal model represents the interaction with a stiff environment, as in [16].

(2) DOB2-CL: A closed-loop DOB architecture using a second order nominal plant, as proposed in [57,59].

[5] The considered low-pass filter has a cut-off frequency of about 20 Hz and is carefully tuned as a trade-off parameter. Lower cut-off frequencies leads to degrade the shape of $W(s)$ leading to a possible mismatch with the nominal model in (15) while higher cut-off frequencies lead to noisy responses. Of course this tuning is system specific since a more accurate force sensing would lead to less noise in the system.

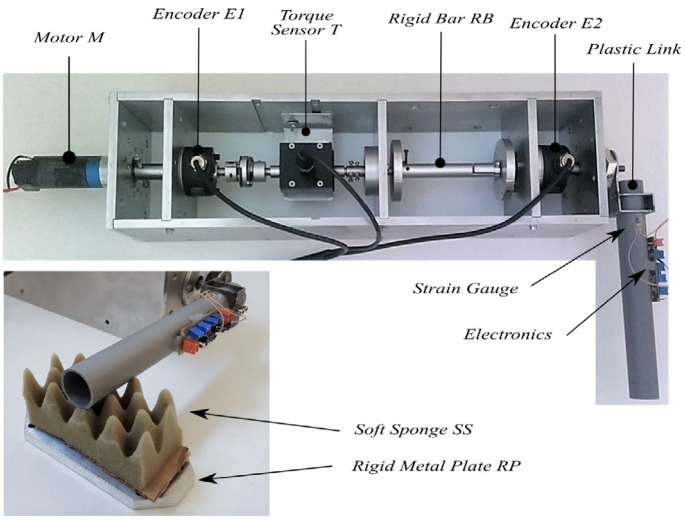

Fig. 12. The experimental setup.

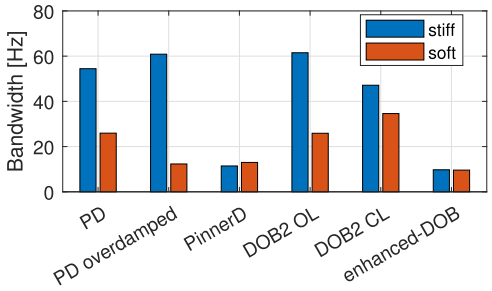

Fig. 13. Graphical representation of estimated bandwidth values for each control architecture tested in stiff and soft environments.

(3) DOB3-OL: An open-loop DOB architecture using a third order nominal plant

$$P_n^{3rd}(s) = \frac{kJs}{J_m J s^3 + J d_m s^2 + [k(J_m + J)]s + k d_m}, \tag{17}$$

representing the interaction through an inertial body, i.e. the link itself, as proposed in [17].

(4) DOB3-CL: A closed-loop DOB architecture using a third order nominal plant. Even if we could not find any existing work related to this specific architecture, it is theoretically meaningful.

To the best of our knowledge, these four architectures represent the complete spectrum of existing DOB-based force control solutions for series elastic systems [16,17]. These controllers are tested and compared with the enhanced-DOB architecture proposed in Section 3.4: a cascaded control schema which includes a inner derivative loop and an outer open-loop DOB, as represented in Fig. 11 where $P_n(s)$ is defined in (15).

The tuning of each control algorithm is reported in Table 1 where ω_q is the location of the cut-off frequency of the $Q(s)$ filter raised up to the maximum value which retains stable and smooth responses. Such cut-off frequency determines the "accuracy" of nominal model inversion, as represented in Fig. 5. In certain cases the nominal model is significantly different from the system dynamics and an aggressive filter $Q(s)$ helps to mitigate such model mismatch. In practice it leads to ameliorate stability outcomes: the DOB action becomes less reactive and more stable. This agrees with previous findings: in case of "poor knowledge of uncertainties" the cutoff frequency of the filter "needs to be decreased to improve the robustness of DOB" [69]. For the DOB2-OL/CL controllers we considered an over-damped tuning, as reported in Table 1, because the critically damped tuning was unstable.

In all our experimental tests existing DOB architectures lead to bad performance robustness or even to instability. The proposed enhanced-DOB architecture seems to be the only one performing suitable robustness to environment changes. In particular, the first two DOB architectures (DOB2-OL/CL) show a similar behavior, stable but not robust to environment variations, leading to undesired overshoots when interacting with the soft sponge, as shown in Fig. 15. Similarity of DOB2-OL and DOB2-CL responses agrees with the results in [16]. The observed sensitivity to environment variations has never been reported before and is probably due to the specific testing scenario: extremely low endpoint inertia. Regarding DOB architectures based on third order nominal models (DOB3-OL/CL), in all our trials they behaved unstably. For those architectures we were not able to find any stable tuning working in both stiff and soft environment conditions. For this reason related responses are not reported. The bottom plots in Fig. 15 show that our enhanced-DOB architecture can finally lead to an improved performance robustness showing almost identical responses in stiff and soft environments. Also, these responses are quite close to the expected behavior (in black). This supports the main theoretical claim of this work: an inner derivative loop helps to reach a dominant dynamics which is less sensitive to environment uncertainties.

4.3. Quantitative comparison

Table 2 reports the estimated bandwidth and the measured maximum overshoot[6] of each controller in stiff and soft environment conditions. Bandwidth estimations have been done using the Matlab System Identification Toolbox and by assuming a suitable order for each closed-loop system. A graphical representation of the estimated bandwidth is reported in Fig. 13. Except for the proposed architectures (PinnerD and enhanced-DOB), it can be observed that for each existing algorithm the bandwidth is significantly higher in stiff environments (about two times

[6] The "measured maximum overshoot" is intended here as the maximum sovra-elongation level in relation to the sweep signal amplitude, measured on the closed-loop responses in Figs. 14 and 15. As the system is excited only between $0 \div 5$ Hz this measure may be different from the classical overshoot definition.

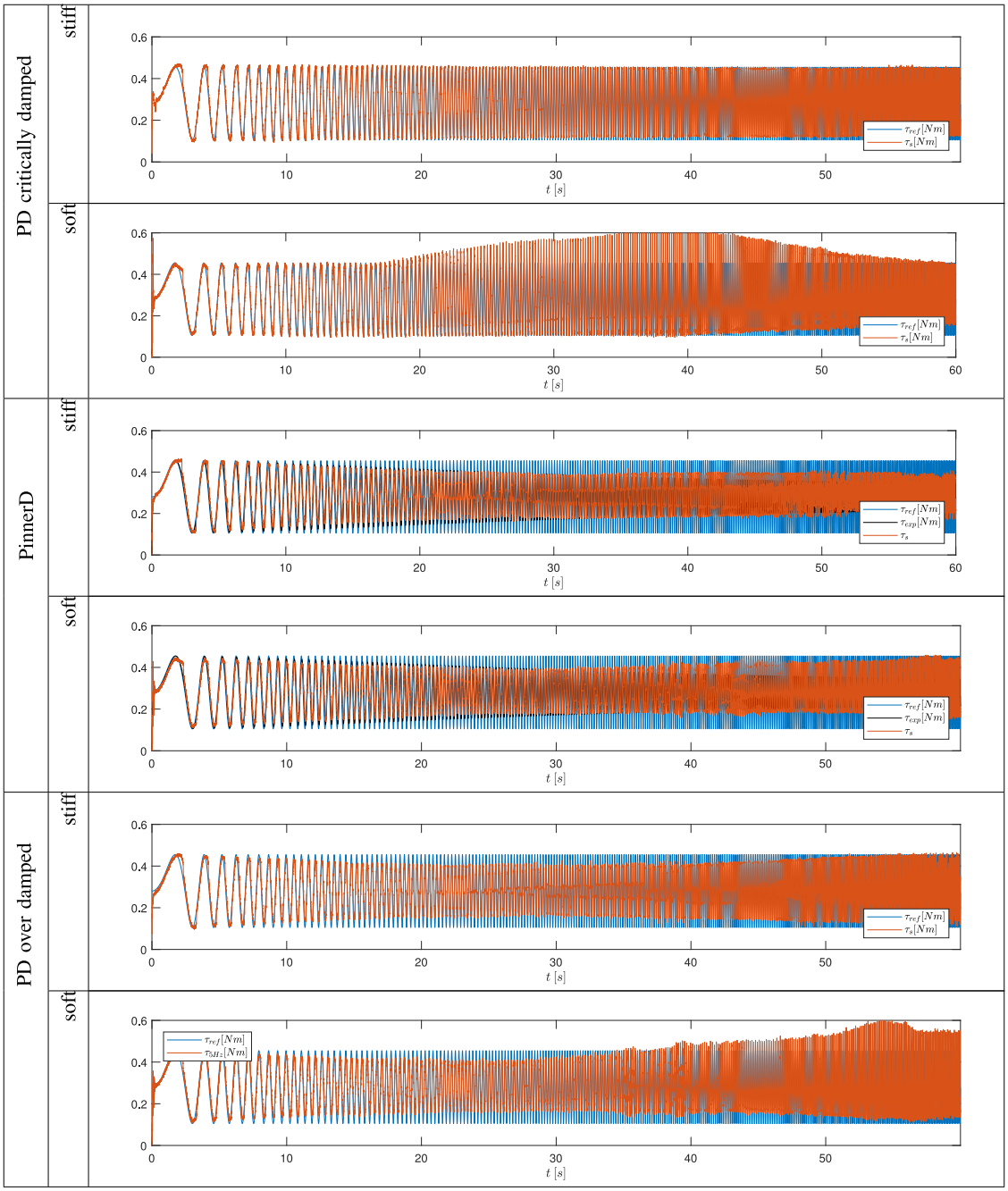

Fig. 14. Force tracking experiments using PD and PinnerD controllers.

higher). The PinnerD architecture leads to dramatically reduce such discrepancy while the proposed enhanced-DOB architecture leads to practically indistinguishably bandwidth values. Similar considerations hold for the maximum overshoot: the proposed architectures are the only ones able to display no overshoot in both stiff and soft environments. According to the considerations in Section 2.3, we do not report any comparison in terms of disturbance estimation, i.e. the signal $\hat{d}$ in Fig. 5. This is because such information would be difficult to interpret. As mentioned before, DOBs consider the uncertainty as additive which in the cases of DOB2-OL/CL and enhanced-DOB has not an intuitive physical meaning.

Table 2
Quantitative comparison.

	Bandwidth estimation		Max. overshoot	
	Stiff Env.	Soft Env.	Stiff Env.	Soft Env.
PD	54.4 Hz	25.9 Hz	4 %	90 %
PD-over damped	60.9 Hz	12.3 Hz	0 %	47 %
PinnerD	11.4 Hz	12.9 Hz	0 %	0 %
DOB2 OL	61.4 Hz	25.9 Hz	1 %	62 %
DOB2 CL	47.1 Hz	34.6 Hz	5 %	48 %
Enhanced-DOB	9.7 Hz	9.6 Hz	0 %	0 %

4.4. Discussion of experimental results

The reported experimental results suggest that force control solutions based on DOBs should be considered with caution when

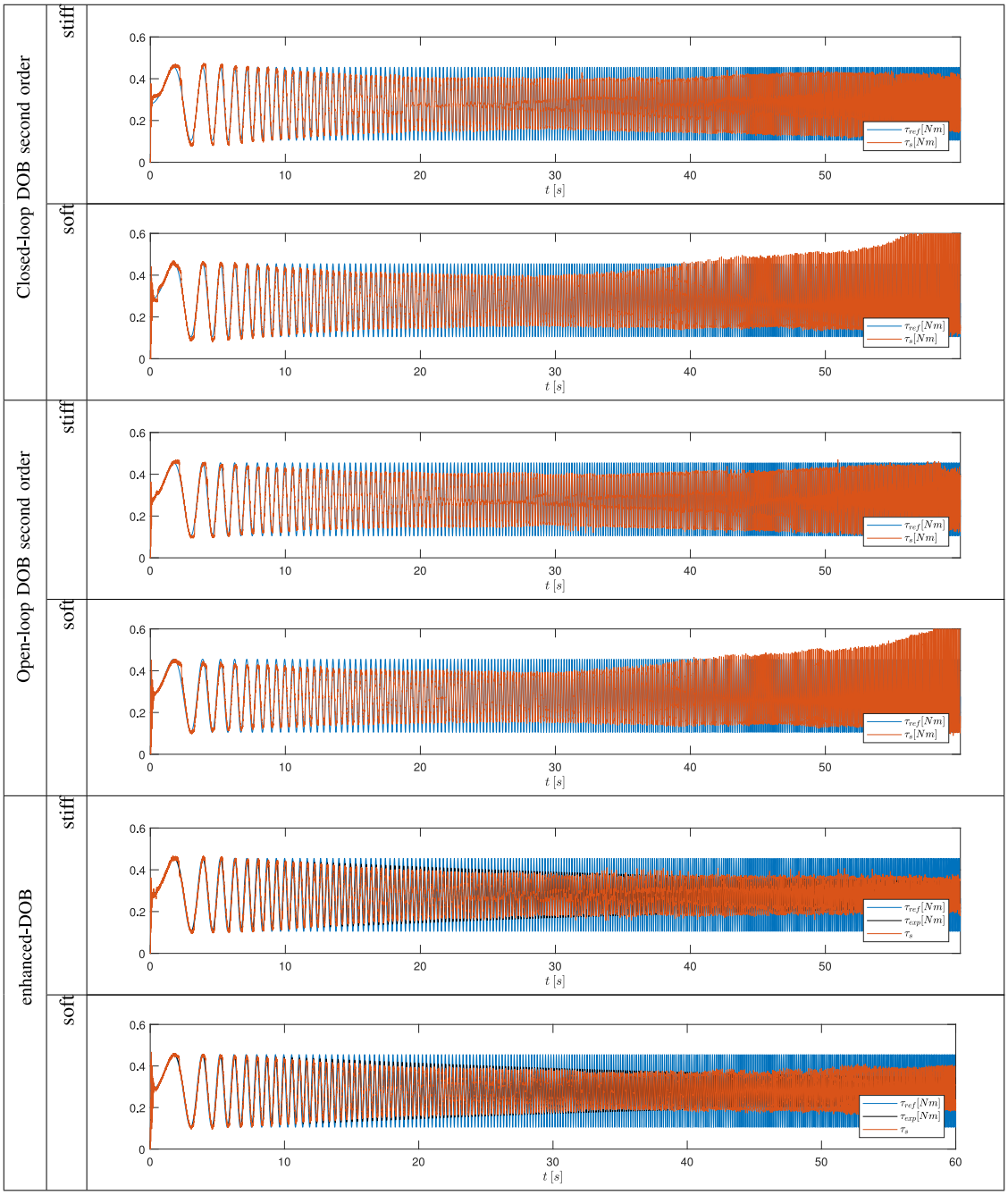

Fig. 15. Force tracking experiments using enhanced-DOB and existing DOB architectures.

the system is too much sensitive to environment dynamics, as in the case of series elastic systems with low end-point inertia. In practice, DOB architectures can deal with environmental variations up to a certain limit. When the sensitivity to such variation becomes too high – and this can be due to a low end-point inertia – existing DOB solutions cannot handle it any more leading to poor robustness and even to unstable behaviors. In those scenarios the proposed robustification based on inner derivative loop can significantly reduce such sensitivity allowing the implementation of a stable and effective outer DOB controller. Also, this work shows that even if a standard PD control can lead to high force control bandwidth, it also leads to bad performance robustness and to unpredictable responses when interacting with unknown environments. This can be highly undesired in certain critical applications. This is the case of robotic surgery where the surgical tool can interact with extremely soft tissues or rigid bones and overshoots or oscillations can be harmful for the patient. As shown in Table 2, the proposed solution is only one able to avoid undesired overshoots both when interacting with extremely soft environments (e.g. soft tissues) or rigid environments (e.g. bones). Instead, PD control can lead to overshoot up to 90% and existing DOB solutions can lead to overshoot of about 50%.

A possible criticism of our approach is the limited bandwidth that we could achieve. In fact, in order to retain stable responses, the admissible proportional gain for the outer controller should not overcome too much the value $k_p = 4$, as reported in Table 1. This limit is not due to the proposed methodology itself

but to some well known issues such as non collocation,[7] limited actuator bandwidth and digitalization effects, which affect our physical implementation [76,78,79]. In our specific case, the actuator bandwidth (i.e. the bandwidth of the current loop) is estimated around 5 kHz, the control process runs at 2 kHz and the gearbox is not highly rigid, possibly leading to non-collocation (the gearbox stiffness is estimated around 500 N m/rad). Among these high frequency dynamics, the non-collocation due to the elastic gearbox dynamics seems to represent the most limiting issue, leading to additional poles below 1 kHz, not considered in our analysis.

5. Conclusions

The theoretical and experimental results presented in this paper motivate the adoption of an inner derivative feedback to improve performance robustness in force control applications. This design has been motivated by the use of lightweight flexible links but it is in principle viable for the entire class of series elastic systems described by model (2)–(4), under the condition that the low frequency poles are not located too close to zero. Theoretical and experimental argumentations have been proposed to support the control strategy including a comparison with state of the art solutions. In particular, we show that where existing DOB architectures fail, a inner derivative loop can significantly reduce the sensitivity to environment uncertainties and can be successfully combined with an outer DOBs. Currently, our group is working at improving the control performance by dealing with non-collocation issues and by using low-noise force sensing solutions.

Declaration of competing interest

The authors declare that they have no known competing financial interests or personal relationships that could have appeared to influence the work reported in this paper.

Data availability

Data will be made available on request.

Acknowledgments

This project has received funding from the European Union's Horizon 2020 programme under grant agreement EUROBENCH n. 779963, from the European Research Council (ERC), under grant agreement ARS n. 742671 "ARS", and has been partially supported by the project of the Italian Ministry of Education, Universities and Research (MIUR) "Dipartimenti di Eccellenza 2018-2022".

References

[1] Rethink Robotics, Baxter Research Robot - Hardware Specifications, 2015, Available http://sdk.rethinkrobotics.com/wiki/Hardware_Specifications (Online).
[2] N.G. Tsagarakis, D.G. Caldwell, F. Negrello, W. Choi, L. Baccelliere, V.G. Loc, J. Noorden, L. Muratore, A. Margan, A. Cardellino, L. Natale, E. Mingo Hoffman, H. Dallali, N. Kashiri, J. Malzahn, J. Lee, P. Kryczka, D. Kanoulas, M. Garabini, M. Catalano, M. Ferrati, V. Varricchio, L. Pallottino, C. Pavan, A. Bicchi, A. Settimi, A. Rocchi, A. Ajoudani, WALK-MAN: A high-performance humanoid platform for realistic environments, J. Field Robotics (2017).

[7] The non-collocation issue arises because the force sensor is not located on the same rigid body where the input force acts. In practice, while the input torque – due to the motor current – is rotating the motor shaft, the force sensor is always located after the gearbox introducing additional higher frequency dynamics due to gearbox [75,76].

[3] G.A. Pratt, M. Williamson, Series Elastic Actuators (Ph.D. dissertation), 1, Massachussetts Institute of Technology, 1995, pp. 399–406, Available http://ieeexplore.ieee.org/xpls/abs_all.jsp?arnumber=525827 (Online).
[4] D.W. Robinson, Design and Analysis of Series Elasticity in Closed-loop Actuator Force Control (Ph.D. dissertation), MIT, 2000.
[5] A. Calanca, R. Muradore, P. Fiorini, A review of algorithms for compliant control of stiff and fixed compliance robots, IEEE/ASME Trans. Mechatronics 21 (2) (2016) 613–624.
[6] S.H. Drake, Using Compliance in lieu of sensory feedback for automatic assembly (Ph.D. dissertation), Massachussetts Institute of Technology, 1978.
[7] T.D. Fazio, D. Seltzer, D. Whitney, The instrumented remote center of compliance, Ind. Robot. 11 (4) (1984) 238–242.
[8] A. Calanca, E. Dimo, R. Vicario, P. Fiorini, M. Serpelloni, G. Legnani, Introducing series elastic links for affordable torque-controlled robots, IEEE Robot. Autom. Lett. 4 (1) (2019) 137–144.
[9] A. Calanca, L. Bettinelli, E. Dimo, R. Vicario, M. Serpelloni, P. Fiorini, Introducing series elastic links, in: M.C. Carrozza, S. Micera, J.L. Pons (Eds.), Wearable Robotics: Challenges and Trends, vol. 22, Springer International Publishing, Pisa, 2019, pp. 465–469.
[10] D. Feliu-Talegon, V. Feliu-Batlle, I. Tejado, B.M. Vinagre, S.H. HosseinNia, Stable force control and contact transition of a single link flexible robot using a fractional-order controller, ISA Trans. 89 (2019) 139–157.
[11] J. Malzahn, R.F. Reinhart, T. Bertram, Dynamics identification of a damped multi elastic link robot arm under gravity, in: Proceedings - IEEE International Conference on Robotics and Automation, 2014.
[12] Y. Li, S.S. Ge, Q. Wei, T. Gan, X. Tao, An online trajectory planning method of a flexible-link manipulator aiming at vibration suppression, IEEE Access 8 (2020) 130616–130632.
[13] T. Haidegger, B. Benyö, L. Kovács, Z. Benyö, Force sensing and force control for surgical robots, in: IFAC Proceedings Volumes (IFAC-PapersOnline), vol. 7, (PART 1) 2009, pp. 401–406.
[14] A. Calanca, E. Dimo, E. Palazzi, L. Luzi, Enhancing force controllability by mechanics in exoskeleton design, Mechatronics 86 (2022).
[15] E. Palazzi, L. Luzi, E. Dimo, M. Meneghetti, R. Vicario, R.F. Luzia, R. Vertechy, A. Calanca, An affordable upper-limb exoskeleton concept for rehabilitation applications, Technologies 10 (1) (2022) 22.
[16] W. Roozing, J. Malzahn, D.G. Caldwell, N.G. Tsagarakis, Comparison of open-loop and closed-loop disturbance observers for series elastic actuators, in: IEEE International Conference on Intelligent Robots and Systems, 2016, pp. 3842–3847.
[17] S. Oh, K. Kong, High precision robust force control of a series elastic actuator, IEEE/ASME Trans. Mechatronics 22 (1) (2017) 71–80.
[18] R.H. Cannon, D.E. Rosenthal, Experiments in control of flexible structures with noncolocated sensors and actuators, J. Guid. Control 3 (3) (1984) 546–553.
[19] R.H. Cannon, E. Schmitz, Initial experiments on the end-point control of a flexible one-link robot, Int. J. Robot. Res. 3 (3) (1984) 62–75.
[20] Y. Sakawa, F. Matsuno, S. Fukushima, Modeling and feedback control of a flexible arm, J. Robot. Syst. 2 (4) (1985) 453–472.
[21] A.G. Chassiakos, G.A. Bekey, Pointwise control of a flexible manipulator arm, IFAC Proc. Vol. 18 (16) (1985) 181–185.
[22] Y. Aoustin, C. Chevallereau, A. Glumineau, C.H. Moog, Experimental results for the end-effector control of a single flexible robotic arm, IEEE Trans. Control Syst. Technol. 2 (4) (1994) 371–381.
[23] M. Shao, Y. Huang, V.V. Silberschmidt, Intelligent manipulator with flexible link and joint: Modeling and vibration control, Shock Vib. 2020 (2020).
[24] X. He, S. Zhang, Y. Ouyang, Q. Fu, Vibration control for a flexible single-link manipulator and its application, IET Control Theory Appl. 14 (7) (2020) 930–938.
[25] P. Chedmail, Y. Aoustin, C. Chevallereau, Modelling and control of flexible robots, Internat. J. Numer. Methods Engrg. 32 (8) (1991) 1595–1619.
[26] B. Siciliano, W.J. Book, A singular perturbation approach to control of lightweight flexible manipulators, Int. J. Robot. Res. 7 (4) (1988) 79–90.
[27] F.L. Lewis, M. Vandegrift, Flexible robot arm control by a feedback linearization/singular perturbation approach, Proc. - IEEE Int. Conf. Robot. Automat. 3 (1993) 729–736.
[28] K.S. Yeung, Y.P. Chen, Regulation of a one-link flexible robot arm using sliding-mode technique, Internat. J. Control 49 (6) (1989) 1965–1978.
[29] A. Shawky, D. Zydek, Y.Z. Elhalwagy, A. Ordys, Modeling and nonlinear control of a flexible-link manipulator, 2013, pp. 9591–9602.
[30] Y. Morita, F. Matsuno, Y. Kobayashi, M. Ikeda, H. Ukai, H. Kando, Lyapunov-based force control of a flexible arm considering bending and torsional deformation, IFAC Proceedings Volumes (IFAC-PapersOnline), vol. 15, (1) IFAC, 2002, pp. 133–138.

[31] W.J. Book, Recursive Lagrangian dynamics of flexible manipulator arms, Int. J. Robot. Res. 3 (3) (1984) 87–101.
[32] A. De Luca, B. Sciliano, Joint-based control of a nonlinear model of a flexible arm, in: Proceedings of the American Control Conference, vol. 88 pt 1-3, American Automatic Control Council, 1988, pp. 935–940.
[33] S.K. Tso, T.W. Yang, W.L. Xu, Z.Q. Sun, Vibration control for a flexible-link robot arm with deflection feedback, Int. J. Non-Linear Mech. 38 (1) (2003) 51–62.
[34] E. Bayo, A Finite-Element Approach To Control the End-Point Motion of a Single-Link Flexible Robot, vol. 4, (1) 1987, pp. 63–75.
[35] G.G. Hastings, W.J. Book, A linear dynamic model for flexible robotic manipulators, IEEE Control Syst. Mag. 7 (1) (1987) 61–64.
[36] E. Barbieri, U. Ozguner, Unconstrained and constrained mode expansions for a flexible slewing link, in: Proceedings of the American Control Conference, vol. 88 pt 1-3, American Automatic Control Council, 1988, pp. 83–88.
[37] D. Wang, M. Vidyasagar, Transfer functions for a single flexible link, IEEE, 1989, pp. 1042–1047.
[38] D. Wang, M. Vidyasagar, Passive control of a single flexible link, IEEE, 1990, pp. 1432–1437.
[39] De Luca Alessandro, Siciliano Bruno, Inversion-based nonlinear control of robot arms with flexible links, J. Guid. Control Dyn. 16 (6) (1993).
[40] H. Geniele, R.V. Patel, K. Khorasani, Control of a flexible-link manipulator, in: Proceedings - IEEE International Conference on Robotics and Automation, vol. 1, 1995, pp. 1217–1222.
[41] R. Franke, J. Malzahn, Vibration control of a multi-link flexible robot arm with Fiber-Bragg-Grating sensors, IEEE Int. Conf. Robot. Automat. (2009).
[42] J. Malzahn, A.S. Phung, R. Franke, H. Frank, T. Bertram, Markerless Visual Vibration Damping of a 3-DOF Flexible Link Robot Arm | VDE Conference Publication | IEEE Xplore, in: ISR / ROBOTIK 2010, 2010.
[43] D. Feliu-Talegon, V. Feliu-Batlle, Passivity-based control of a single-link flexible manipulator using fractional controllers, Nonlinear Dynam. 95 (3) (2019) 2415–2441.
[44] A. Garcia, V. Feliu, A. García, V. Feliu, Force control of a single-link flexible robot based on a collision detection mechanism, IEEE Proc. D 147 (6) (2000) 588–595.
[45] J. Malzahn, T. Bertram, Collision detection and reaction for a multi-elastic-link robot arm, in: IFAC Proceedings Volumes (IFAC-PapersOnline), vol. 19, 2014, pp. 320–325.
[46] J. Malzahn, R. Schloss, T. Bertram, Link elasticity exploited for payload estimation and force control, IEEE Int. Conf. Intell. Robots Syst. 2015-Decem (2015) 1508–1513.
[47] D. Feliu-Talegon, V. Feliu-Batlle, A fractional-order controller for single-link flexible robots robust to sensor disturbances, IFAC-PapersOnLine 50 (1) (2017) 6043–6048.
[48] D. Feliu-Talegon, V. Feliu-Batlle, Control of very lightweight 2-DOF single-link flexible robots robust to strain gauge sensor disturbances: A fractional-order approach, IEEE Trans. Control Syst. Technol. (2021) 1–16.
[49] Feliua Vicente, Pereirab Emiliano, M. Díaz Iván, Passivity-based control of single-link flexible manipulators using a linear strain feedback, Mech. Mach. Theory J. (2014).
[50] L.Y. Liu, H.C. Lin, Tip-contact force control of a single-link flexible arm using feedback and parallel compensation approach, Robotica 31 (5) (2013) 825–835.
[51] A. Calanca, P. Fiorini, On the role of compliance in force control, in: E. Menegatti, N. Michael, K. Berns, H. Yamaguchi (Eds.), Advances in Intelligent Systems and Computing, 302, Springer International Publishing, Padova, Italy, 2016, pp. 1243–1255.
[52] A. Calanca, P. Fiorini, A rationale for acceleration feedback in force control of series elastic actuators, IEEE Trans. Robot. 34 (1) (2018) 48–61.
[53] R. Volpe, P. Khosla, Theoretical and experimental investigation of explicit force control strategies for manipulators, IEEE Trans. Automat. Control 38 (11) (1993) 1634–1650.
[54] N. Mandal, S. Payandeh, Force control strategies for compliant and stiff contact: an experimental study, Proc. IEEE Int. Conf. Syst. Man Cybern. 2 (1994) 1285–1290.
[55] B. Brogliato, B. Maschke, R. Lozano, O. Egeland, Dissipative systems analysis and control: Theory and applications, Springer-Verlag London, 2007, p. XIV, 579.
[56] T. Boaventura, J. Buchli, Coupled Systems Analyses for High-performance Robust Force Control of Wearable Robots, in: IEEE RAS/EMBS International Conference on Biomedical Robotics and Biomechatronics, 2016, pp. 1021–1026.
[57] K. Kong, S. Member, J. Bae, Control of rotary series elastic actuator for ideal force-mode actuation in human-robot interaction applications, IEEE/ASME Trans. Mechatronics 14 (1) (2009) 105–118.
[58] H. Yu, S. Huang, G. Chen, Y. Pan, Z. Guo, Human-robot interaction control of rehabilitation robots with series elastic actuators, IEEE Trans. Robot. 31 (5) (2015) 1089–1100.
[59] N. Paine, J.S. Mehling, J. Holley, N.A. Radford, G. Johnson, C.L. Fok, L. Sentis, Actuator control for the NASA-JSC valkyrie humanoid robot: A decoupled dynamics approach for torque control of series elastic robots, J. Field Robotics 32 (3) (2015) 378–396.
[60] T. Boaventura, M. Focchi, M. Frigerio, J. Buchli, C. Semini, G.a. Medrano-Cerda, D.G. Caldwell, On the role of load motion compensation in high-performance force control, in: 2012 IEEE/RSJ International Conference on Intelligent Robots and Systems, Ieee, 2012, pp. 4066–4071.
[61] J. Bae, K. Kong, M. Tomizuka, Gait Phase-Based Smoothed Sliding Mode Control for a Rotary Series Elastic Actuator Installed on the Knee Joint, in: American Control Conference, Marriott Waterfront, Baltimore, MD, USA, 2010, pp. 6030–6035.
[62] M. Wang, L. Sun, W. Yin, S. Dong, J. Liu, A novel sliding mode control for series elastic actuator torque tracking with an extended disturbance observer, in: 2015 IEEE International Conference on Robotics and Biomimetics (ROBIO), (June) 2015, pp. 2407–2412.
[63] D.P. Losey, A. Erwin, C.G. McDonald, F. Sergi, M.K. O'Malley, A time domain approach to control of series elastic actuators: Adaptive torque and passivity-based impedance control, IEEE/ASME Trans. Mechatronics 21 (4) (2016) 2085–2096.
[64] K.D. Kaya, L. Çetin, Adaptive state feedback controller design for a rotary series elastic actuator, Trans. Inst. Meas. Control 39 (2017) 61–74.
[65] A. Calanca, P. Fiorini, Understanding environment-adaptive force control of series elastic actuators, IEEE/ASME Trans. Mechatronics 23 (1) (2018) 413–423.
[66] A. Calanca, P. Fiorini, Impedance control of series elastic actuators based on well-defined force dynamics, Robot. Auton. Syst. 96 (2017) 81–92.
[67] N. Yu, W. Zou, Y. Sun, Passivity guaranteed stiffness control with multiple frequency band specifications for a cable-driven series elastic actuator, Mech. Syst. Signal Process. (2019).
[68] M. Tomizuka, Motion controller design for high-accuracy positioning systems, IEEE Trans. Ind. Electron. 43 (1) (1996) 48–55.
[69] K. Kong, M. Tomizuka, Nominal model manipulation for enhancement of stability robustness for disturbance observer-based control systems, Int. J. Control Autom. Syst. 11 (1) (2013) 12–20.
[70] D. Whitney, Force Feedback Control of Manipulator Fine Motions, Trans. ASME J. Dyn. Syst. Measurement Control 99 (2) (1977) 91–97.
[71] G. Markus, M. Roman, U. Konigorski, Model Based Control of Series Elastic Actuators, in: IEEE RAS/EMBS International Conference on Biomedical Robotics and Biomechatronics, (3) Roma, Italy, 2012, pp. 538–543.
[72] A. Calanca, L. Capisani, P. Fiorini, Robust force control of series elastic actuators, Actuators, Special Issue on Soft Actuators 3 (3) (2014) 182–204.
[73] G. Aguirre-Ollinger, U. Nagarajan, A. Goswami, An admittance shaping controller for exoskeleton assistance of the lower extremities, Auton. Robots 40 (4) (2016) 701–728.
[74] D. Whitney, Historical perspective and state of the art in robot force control, Int. J. Robot. Res. (1987) 262–268.
[75] S. Eppinger, W. Seering, On dynamic models of robot force control, in: Proceedings. 1986 IEEE International Conference on Robotics and Automation, vol. 3, Institute of Electrical and Electronics Engineers, 1986, pp. 29–34.
[76] S. Eppinger, W. Seering, Understanding bandwidth limitations in robot force control, in: Proceedings. 1987 IEEE International Conference on Robotics and Automation, vol. 4, 1987, pp. 904–909.
[77] A. Calanca, L.M.L. Capisani, A. Ferrara, L. Magnani, MIMO closed loop identification of an industrial robot, IEEE Trans. Control Syst. Technol. 19 (5) (2011) 1214–1224.
[78] J.E. Colgate, G.G. Schenkel, Passivity of a class of sampled-data systems: Application to haptic interfaces, J. Robot. Syst. 14 (1) (1997) 37–47.
[79] S. Buerger, N. Hogan, Relaxing passivity for human-robot interaction, in: 2006 IEEE/RSJ International Conference on Intelligent Robots and Systems, Ieee, 2006, pp. 4570–4575.

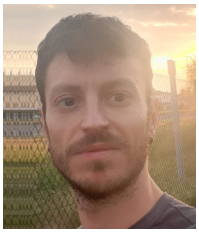

Andrea Calanca received the master degree in Computer Engineering cum laude from the University of Pavia in 2006. For some years he worked in companies as software, DSP and control engineer and in 2009 he joined the Altair Robotics Laboratory at University of Verona, where he received the Ph.D. in 2014 under the supervision of Prof. Paolo Fiorini. He is currently working at University of Verona as a research associate. He currently leads a team doing research on force control, elastic actuators, flexible links, emg-based control and affordable robotics. A special focus is in control technologies for advanced physical humanrobot interaction including the control of assistive and rehabilitation devices.

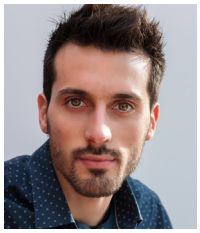

Enrico Sartori received the master degree in Computer Science at the University of Verona in 2018. During his studies he joined the Altair Robotics Laboratory where he focused on robotics for medical applications, from surgery to rehabilitation, under the supervision of Prof. Paolo Fiorini and Prof. Andrea Calanca. In 2019, he joined Franka Emika GmbH, leading company in the field of compliant industrial robotics, where he currently works as Control and Software Engineer.

Bogdan Maris received a degree in Mathematics from the 'Babes-Bolyai' University, Cluj-Napoca, Romania, the Laurea in Computer Science and the Ph.D. degree in Computer Science from the University of Verona, Italy. Since 2008 he has been a Research Fellow with the ALTAIR Robotics Laboratory and since 2018 he is an Assistant Professor at the Department of Computer Science, University of Verona, Italy. His research interests includes robotics, human robot interaction with a particular focus on medical robotics.